Nuclear heparanase-1 activity suppresses melanoma progression via its DNA-binding affinity

Yang, Yi ; Gorzelanny, Christian ; Bauer, A T ; Halter, Natalia ; Komljenovic, D ; Bäuerle, T ; Borsig, Lubor ; Roblek, Marko ; Schneider, Stefan W

Abstract: Heparanase-1 (HPSE) plays a pivotal role in structural remodeling of the ECM and glycocalyx thus conferring protumorigenic, proangiogenic and prometastatic properties to many cancer entities. In addition to its extracellular function, recent studies suggest an intracellular activity of HPSE with a largely unknown significance during tumor progression. Therefore, we investigated the relevance of HPSE duality in malignant melanoma in vitro as well as in mouse melanoma models basing on the intradermal injection of transfected melanoma cells. In line with its extracellular action, HPSE-deficiency led to a reduced shedding of the glycocalyx accompanied by a reduced availability of VEGF affecting tumor growth and vascularization. In contrast, we measured an elevated expression of the protumorigenic factors pentraxin-3, tissue factor, TNF-and most prominently MMP-9 upon HPSE knockdown. In vivo, HPSE-deficiency was related to increased lymph node metastasis. While inhibition of its extracellular function heparin was unable to block the gene regulatory impact of HPSE we proposed an intracellular mechanism. Immunostainings revealed a counter-staining of HPSE and NF- B in the nucleus suggesting a close relationship between both proteins. This finding was further supported by the discovery of a direct charge-driven molecular interaction between HPSE and DNA by using atomic force microscopy and a co-precipitation approach. Our findings are novel and point towards a dual identity of HPSE in malignant melanoma with a protumorigenic extracellular activity and a tumor suppressive nuclear action. Identification of molecular strategies to shuttle extracellular HPSE into the nuclei of cancer cells envisions new therapeutic options.

DOI: https://doi.org/10.1038/onc.2015.40

Nuclear Heparanase-1 Activity Suppresses Melanoma Progression via its DNA Binding Affinity

Yi Yang[1,†], Christian Gorzelanny[1,†], Alexander T. Bauer[1], Natalia Halter[1], Dorde Komljenovic[2], Tobias Bäuerle[3], Lubor Borsig[4], Marko Roblek[4] and Stefan W. Schneider[1]*

[1] Department of Dermatology, Experimental Dermatology, Medical Faculty Mannheim, Heidelberg University, Theodor-Kutzer-Ufer 1-3, 68167 Mannheim, Germany

[2] Division of Medical Physics in Radiology, German Cancer Research Center (DKFZ), Im Neuenheimer Feld 280, 69120 Heidelberg, Germany

[3] Institute of Radiology, University Hospital Erlangen, Maximiliansplatz 1, 91054 Erlangen, Germany

[4] Institute of Physiology, University of Zürich and Zürich Center for Integrative Human Physiology, CH-8057 Zürich, Switzerland

[†] These authors contributed equally to this work.

* **Corresponding author**: Stefan W. Schneider, Department of Dermatology, Experimental Dermatology, Medical Faculty Mannheim, Heidelberg University, Theodor-Kutzer-Ufer 1-3, 68167 Mannheim, Germany; Phone: +49-(0)621-383 6901; Fax: +49-(0)621-383 6903; Email: stefan.schneider@medma.uni-heidelberg.de

Running title: Nuclear Heparanase-1 Activity in Melanoma

Financial support: This work was supported by the Deutsche Forschungsgemeinschaft within the SFB/Transregio 23 (project A9 to S.W.S).

Abstract

Heparanase-1 (HPSE) plays a pivotal role in structural remodeling of the ECM and glycocalyx thus conferring protumorigenic, proangiogenic and prometastatic properties to many cancer entities. In addition to its extracellular function, recent studies suggest an intracellular activity of HPSE with a largely unknown significance during tumor progression. Therefore, we investigated the relevance of HPSE duality in malignant melanoma *in vitro* as well as in mouse melanoma models basing on the intradermal injection of transfected melanoma cells. In line with its extracellular action, HPSE-deficiency led to a reduced shedding of the glycocalyx accompanied by a reduced availability of VEGF affecting tumor growth and vascularization. In contrast, we measured an elevated expression of the protumorigenic factors pentraxin-3, tissue factor, TNF-α and most prominently MMP-9 upon HPSE knockdown. *In vivo*, HPSE-deficiency was related to increased lymph node metastasis. While inhibition of its extracellular function heparin was unable to block the gene regulatory impact of HPSE we proposed an intracellular mechanism. Immunostainings revealed a counter-staining of HPSE and NF-κB in the nucleus suggesting a close relationship between both proteins. This finding was further supported by the discovery of a direct charge-driven molecular interaction between HPSE and DNA by using atomic force microscopy and a co-precipitation approach. Our findings are novel and point towards a dual identity of HPSE in malignant melanoma with a protumorigenic extracellular activity and a tumor suppressive nuclear action. Identification of molecular strategies to shuttle extracellular HPSE into the nuclei of cancer cells envisions new therapeutic options.

Keywords: melanoma, metastasis, angiogenesis, matrix metalloproteinase, NF kappaB

Introduction

As the only known enzyme for heparan sulfate (HS) degradation from extracellular matrix (ECM), heparanase-1 (HPSE) mediates the release of HS-bound growth factors (i.e., vascular endothelial growth factor (VEGF)), thus promoting endothelial cell activation and angiogenic responses [1, 2], a process that is further supported by HPSE-generated fragments of HS [3]. Besides its extracellular action, HPSE has been discovered to exert nuclear action by shedding syndecan-1 in the nuclei of myeloma cells [4]. Loss of nuclear syndecan-1 interferes with gene transcription via enhanced histone acetylation and enhanced extracellular signal-regulated kinase (ERK) activation which including the up-regulation of matrix metalloproteinase 9 (MMP-9) [4-6]. MMP-9 is known to be transcriptionally regulated by NF-κB signaling pathway [7, 8]. Notably, other reports suggest a connection between HPSE and the regulation of NF-κB related genes [9-12]. In addition to the enzymatic functions, non-enzymatic activity of HPSE enhances Akt signaling and stimulates phosphatidylinositol 3-kinase (PI3K)-dependent migration and invasion of endothelial cells [13] and up-regulates the expression of VEGF in several tumor cell lines via the Src pathway [14]. These findings suggest that the capacity of HPSE in regulating cell signaling and gene transcription depends on both enzymatic and non-enzymatic activities as well as on its extracellular and/or intracellular localization.

Although the additional ongoing mechanisms are currently discussed, the contribution of HPSE in tumor progression is broadly investigated. Up-regulation of HPSE exerts protumorigenic properties at early stages of tumor initiation and facilitates tumor growth, angiogenesis and metastasis in many human cancer entities [15-17]. By cooperating with Ras mutation, HPSE could even promote the development of skin malignancy [17]. However, in relation to the cytosolic HPSE, an increased amount of nuclear HPSE is associated with a decreased tumor growth in and an increased survival of patients suffering from head and neck tumors [18]. This finding appears to be counterintuitive to the accepted pro-malignant action of

HPSE and demonstrates a significant impact of nuclear HPSE on the progressivity of cancer cells. Although recent data consistently demonstrate reduced invasive properties upon HPSE down-regulation in melanoma cells [19-21], the contribution and underlying molecular mechanisms of nuclear HPSE in human malignant melanoma remains unexplored. Therefore, the present study aims to investigate the impact of HPSE, especially its nuclear activity on the malignant behaviour of melanoma.

To investigate the regulatory mechanisms of HPSE in tumor progression of malignant melanoma we evaluated the invasive properties of several melanoma cell lines *in vitro* as well as *in vivo*. Invasive properties of melanoma cells were related to the regulation of VEGF, MMPs and the NF-κB signaling pathway [22, 23].

Results

Knockdown of HPSE reduces melanoma cell invasive capacity

Related to our previous work we compared three human melanoma cell lines (BLM, MV3 and IGR37) *in vitro* [22]. BLM and MV3 cells express high levels of HPSE. Comparable less amounts of HPSE were produced by IGR37 cells which were therefore used as a control cell line (Fig. 1A) To proof the cell-specific function of HPSE we additionally attenuated HPSE expression by applying HPSE specific siRNA (siHPSE). Knockdown efficiency controlled with immunoblotting and RT-qPCR was ~ 70% in comparison to cells transfected with non-targeting control siRNA (siCon) (Fig. 1A-C). To evaluate the progression of human malignant melanoma cells we applied a previously established electrophysiological invasion assay [24, 25]. The assay is based on the tumor cell-induced breakdown of an electrically tight epithelium recorded by measurements of trans-epithelial electrical resistance (TEER). Low TEER value corresponds to high invasive potential. Physical separation of the invading cells and the epithelium limits the system variables to secreted factors (schematic sketch in Figure 1D). In comparison to the siCon group, knockdown of HPSE in BLM and MV3 cells resulted in a delayed TEER breakdown. No significant differences were discovered in the control cell line, IGR37 (Fig. 1E). Time courses of TEER experiments have been summarized as bar diagram and are displayed in Fig. 1F. TEER data suggest that HPSE is implicated in the invasive capacity of human malignant melanoma. However, invasion was only delayed but not completely abolished suggesting the contribution of other secreted factors such as MMPs.

Knockdown of HPSE enhances the expression of MMP but reduces the availability of VEGF

We previously demonstrated that MMP-2 and MMP-9 secreted from melanoma cells are strongly involved in the breakdown of TEER [25, 26]. Therefore, we analyzed the secreted amounts of both proteinases in supernatants of melanoma cells by gelatin gel zymography.

Figure 2 A and B show a dramatically increased MMP-9 activity in the supernatants of HPSE deficient BLM and MV3 cells. In contrast, MMP-2 activity was not affected by HPSE knockdown (Fig. 2C, D). No MMP-9 and only a slightly decreased MMP-2 activity were detected in the control cell line IGR37 after HPSE silencing. To prove whether the increased amounts of MMP-9 found in the supernatants of BLM and MV3 cell are related to an elevated gene expression level we performed quantitative real-time PCR. In accordance with our gel zymography data, we found a strongly increased MMP-9 expression in HPSE-deficient BLM and MV3 cells. Notably, these cells showed also an increased expression of MMP-2. Expression levels of neither MMP-9 nor MMP-2 were affected in IGR37 cells upon HPSE knockdown (Fig. 2E, F).

HPSE is known to release the surface-bound VEGF by shedding the cellular glycocalyx as well as the ECM [1]. More recently, we could demonstrate that VEGF availability is also related to the extracellular activity of MMP-9 and MMP-2 [22, 27]. In the present experimental model, the VEGF concentration was significantly attenuated in the supernatants of BLM and MV3 siHPSE cells. No significant difference was found in IGR37 cells (Fig. 2G). In line with a decreased amount of VEGF in the supernatants, we detected an increased retention of VEGF within the glycocalyx of BLM and MV3 cells applying immunostainings (Fig. 2H). Although a slight decrease of VEGF mRNA level was found in BLM siHPSE cells, VEGF expression levels were not affected in MV3 or IGR37 cells (Supplementary Fig. S1A). These data suggest that the regulative impact of HPSE on VEGF in melanoma cells is mostly related to the extracellular activity of HPSE which in turn leads to a reduced availability of VEGF upon HPSE deficiency.

To control whether the up-regulation of MMPs in human melanoma cells after HPSE knockdown was directly related to the shedding of the ECM, we blocked the extracellular action of HPSE with unfractionated heparin (UFH). Heparin is known to inhibit the enzymatic activity of HPSE and to block VEGF [28, 29]. In contrast to HPSE silencing, UFH treatment was

not potent to up-regulate MMP-9 nor MMP-2 in none of the three human melanoma cell lines (Supplementary Fig. S1B, C). Further control experiments excluded an expressional regulation of HPSE (Supplementary Fig. S1D-F).

Taken together, these data suggest a dual role of HPSE in human melanoma cells comprising an intrinsic gene regulatory effect on the one hand and an extracellular activity of HPSE on the other hand. While the availability of VEGF in the supernatant depends mainly on the extracellular activity of HPSE, the up-regulation of MMPs appears to be independent of the extracellular activity of HPSE but to be more related to an intrinsic regulation of gene expression.

HPSE is associated with Nuclear Factor kappa B signaling pathway

The gelatinase MMP-9 is known to be transcriptionally regulated by NF-κB [7, 8]. Interestingly, HPSE has been already linked to NF-κB activation by the descriptive analysis of human tumor tissues [9]. These promote us to hypothesize a potential molecular connection between HPSE and the NF-κB signaling pathway. To this end, we next analyzed whether HPSE alters the expression of other NF-κB-related genes. In comparison to the control cell line IGR37, RT-qPCR analysis revealed a significantly increased expression of TNF-α, tissue factor (TF) and pentraxin-3 (PTX-3) in BLM and MV3 cells upon HPSE knockdown (Fig. 3A-C). As NF-κB is transferred from the cytoplasm into the nucleus after activation we further studied the distribution of the NF-κB subunit p65 by immunostaining and western blot analysis. In line with an elevated MMP-9 expression and other NF-κB-related genes, the knockdown of HPSE resulted in a significantly increased amount of nuclear NF-κB in BLM and MV3 cells suggesting a molecular linkage between HPSE and NF-κB (Fig. 3D and E). Immunostainings of HPSE and MMP-9 were performed as control experiments. Reduced HPSE and increased MMP-9 staining were observed in the HPSE down-regulated cells (Supplementary Fig S2A, B). It is intriguingly to note that HPSE localized mainly in the nuclei rather than in the

cytoplasm of human melanoma cells. We further performed control experiments with recombinant human TNF-α, a potent activator of the NF-κB signal transduction pathway [30]. Immunostaining and western blot analysis identified a translocalization of NF-κB from the cytoplasm to the cell nucleus upon TNF-α treatment (Supplementary Fig S2C, D). In analogy to the HPSE knockdown experiments (Fig. 2), stimulation of BLM and MV3 cells with TNF-α (1, 5, 10 ng/ml) also resulted in a dose-dependent increase of the MMP-9 expression (Supplementary Fig. S3A-C). Interestingly, our data demonstrated a significantly decreased HPSE expression upon TNF-α treatment (Supplementary Fig. S3D-F). Taken together, these data indicate a close relationship between HPSE and NF-κB.

Transcriptional regulation is interfered by the interaction between HPSE and DNA

Due to the fact that heparan sulfate (HS), the natural substrate of HPSE, and DNA are both strongly negatively charged polyelectrolytes, we hypothesized a charge-driven interaction between HPSE and DNA in the cell nucleus by which it could potentially interfere with the NF-κB signaling pathway. To prove this, we purified genomic DNA from melanoma cell nuclear extracts by alcoholic precipitation. Corresponding western blot analysis indicated a co-precipitation of HPSE upon low salt conditions (0.1 M NaCl) (Fig. 4A). In contrast, HPSE was not detected after eluting DNA-bound proteins with high amount of salt (5 M NaCl) prior to the precipitation. High amounts of salt are known to efficiently screen electrostatic forces explaining the dissociation of DNA-bound HPSE.

The interaction between HPSE and DNA was further confirmed by atomic force microscopy (AFM), investigating the interaction between recombinant human HPSE with plasmid DNA. In reference to previous studies, a molecular interaction would be displayed by the formation of aggregates [31]. Representative images of single HPSE molecules (Fig. 4B) and circular plasmid DNA (Fig. 4C) are shown. Co-incubation of HPSE and DNA at different molar ratios resulted in the different formation of protein-DNA complexes. While we partially visualized

free DNA strands at low concentrations of HPSE (Fig. 4D), a saturated complex formation of DNA was apparent at high concentrations of HPSE (Fig. 4E). In control experiments, by using bovine serum albumin (BSA) instead of HPSE, no significant interaction between BSA and DNA was found (Supplementary Fig. S4).

The assumed charge-driven interaction suggests that the binding between HPSE and DNA is non-specific. To further test the degree of specificity, we performed a solid-phase binding assay. For this purpose, binding of biotin-tagged NF-κB consensus oligonucleotides or randomized oligonucleotides to surface immobilized HPSE was analysed. BSA was used as a negative control while positively charged poly-L-lysine served as a positive control. Compared to BSA, binding of oligonucleotides to HPSE was markedly increased indicated by 4-fold higher OD-values confirming the interaction between HPSE and DNA (Fig. 4F). Notably, DNA binding is not strongly dependent on the sequence as we could not measure a significant difference between the NF-κB consensus oligonucleotides or the randomized oligonucleotides (Fig. 4F).

Taken together, these data suggest that expressional regulation of MMPs and related factors is due to a direct interference on the gene transcriptional level by nuclear HPSE-DNA interaction. As the binding capacity is non-specific, other signaling pathways apart from NF-κB might also be involved.

Down-regulation of HPSE inhibits tumor xenograft growth and angiogenesis but induces MMP activity

For an *in vivo* proof of our *in vitro* findings, we next performed experiments in mouse model. Intradermal injection of stable siHPSE or siCon transfected B16F10 cells (7.5×10^5) into the dorsal skin of C57BL/6 mice led to the formation of intact tumors with lymphatic tumor progression resembling the clinical situation of melanoma patients. Knockdown efficiency of HPSE was ~75% (Supplementary Fig. S5A). The time-dependent tumor growth was followed

for 30 days. Tumor xenografts produced by siHPSE cells represented a slower growth rate compared to control xenografts which was in line with the delayed TEER breakdown (Fig. 5A). Of note, cell viability was not affected by the knockdown of HPSE (Supplementary Fig. S5B). To confirm the functionality of our HPSE-deficient cell lines, we injected B16F10 melanoma cells into the tail veins of mice and assess the distant lung metastasis as previously reported [32]. In line with literature we found a marked reduction of lung metastatic foci in mice receiving siHPSE cells (Supplementary Fig. S5C).

As our *in vitro* data demonstrated the involvement of HPSE extracellular activity in VEGF release from cell surface ECM, we hypothesized an enhanced immobilization of VEGF in tumor section. To test this, we immunostained VEGF in tumor sections and indeed an increased VEGF fluorescence intensity was observed upon HPSE knockdown (Fig. 5B). To understand the impact of VEGF in our model, we analyzed the angiogenesis in tumors. Representative mosaic images of CD31-immunostained-cryosection composed of 48 consecutive microscopic fields are presented in Figure 5C. Quantitative analysis of the average blood vessel amount of every single microscopic field in each group (at least 12 mosiac images from 6 xenografts per group) revealed a 2-fold decreased microvessel density in tumors produced by siHPSE transfected cells versus siCon cells (Fig. 5D) suggesting a reduced of availability of VEGF [33]. Previous report demonstrated that elevated levels of VEGF results in an abnormal and impaired functionality of tumor vessels. Correspondingly, reduction of VEGF in tumor tissue, e.g. by an anti-angiogenic therapy is known to result in a normalization of the vasculature as indicated by an increased blood flow [34]. In accordance with this and indicative for a reduced availability of VEGF, we found by dynamic contrast enhanced magnetic resonance imaging (DCE-MRI) an increased blood volume in tumors which were generated by HPSE-deficient B16F10 cells (Fig. 5E).

However, in contrast to a decreased tumor growth and an anti-angiogenic effect, we observed a significant increase in lymph node metastasis (Fig. 6A). While 4 of the total 7 mice

developed lymph node metastasis in the siCon group, the corresponding number of metastatic mice increased to 6 in the siHPSE group. In line with that, we found a clear tendency of a reduced survival rate in mice bearing tumors of HPSE-deficient B16F10 cells (Fig. 6B). Since our *in vitro* data reflected that melanoma progression might be related to an increased expression of MMPs, we next performed gelatine based *in situ* zymography to assess MMP activities in tumor tissues. Compared to siCon group, tumors in siHPSE group exhibited significantly higher MMP activities (Fig. 6C). As *in situ* zymography is unable to distinguish between MMP-2 and MMP-9, we performed RT-qPCR based on B16F10 cells. A 2.5 ± 0.4-fold increase of MMP-2 mRNA level was found in siHPSE transfected cells compared to control group (Fig. 6D).

In order to unify our *in vivo* model with our *in vitro* data, we repeated our mouse experiments with *ret* transgenic melanoma cells as PCR result revealed a dramatic increase of MMP-9 mRNA level in HPSE knockdown cells (Supplementary Fig. S6A). In consistent with the data from B16F10 tumors, *ret* siHPSE tumors represented a slower growth rate compared to control xenografts, together with an attenuated tumor angiogenesis (Supplementary Fig. S6B-D). Likewise, increased amount of mice with metastatic lymph nodes were identified in the siHPSE group (Supplementary Fig. S6E).

Since our *in vitro* results point towards the regulation of NF-κB controlled genes through the binding of DNA, we further investigated the effect of HPSE on NF-κB signaling *in vivo*. However, no significant differences of NF-κB nuclear translocalization were identified in B16F10 tumor cryosections (Fig. 6E). As MMP-2 instead of MMP-9 was regulated in B16F10 cells, we therefore performed a protein profiler array by using *ret* tumor tissue lysates to unify our model. It is interesting to note that although some proteins were down-regulated in siHPSE tumor lysates, over 20 proteins including TNF-α, pro-MMP-9 were up-regulated (Supplementary Fig. S6F). These data indicate that NF-κB pathway is indeed interfered in our model although other pathways may be also involved.

Taken together, these results demonstate that HPSE knockdown inhibits tumor growth and angiogesis but induces MMP activity and expression *in vivo*, confirming our *in vitro* findings.

Discussion

Prometastatic activities of HPSE have been observed in several human malignancies, including colorectal carcinoma, cervical cancer and multiple myeloma [35-37]. However, the relevance of the more recently discovered gene regulatory functions of nuclear HPSE [5, 6] remains uninvestigated in melanoma progression and thus the motivation of our study.

The three human melanoma cell lines used in this study represent cells with different basic expression levels of HPSE, high in BLM and MV3 cells but low in IGR37 cells (Fig. 1A). In the first set of experiments we investigated the invasive properties of all three cell lines with an electrophysiological cell-based invasion assay previously established in our laboratory [24, 25]. One of the key features of this assay is the high sensitivity to evaluate very early steps of invasion [26]. Although the invasive behaviour of the three cell lines was comparable in siCon cells, we found that knockdown of HPSE attenuates the invasive properties in BLM and MV3 cells as indicated by a delayed decrease of electrical resistance (Fig. 1E). In line with the low expression level, knockdown of HPSE was with no significant effects in IGR37 cells, pointing towards cell type-dependent invasion behaviours. Notably, TEER breakdown was only delayed but not completely abolished suggesting the contribution of other secreted factors.

MMPs are deeply connected to physiological and pathophysiological processes related to extracellular matrix modification as it occurs during cancer cell spreading [38]. As we have identified in previous studies that MMP-1, MMP-2, MMP-9 [25, 26] and VEGF [22] are crucially involved in the progression of melanoma cells, we further analyzed the release and expression of MMPs and VEGF upon HPSE knockdown. Surprisingly, we found a strong up-regulation of MMP-9 in BLM and MV3 cells upon HPSE knockdown which might be the explanation for the delayed TEER breakdown (Fig. 2A, E). An elevated enzymatic activity of HPSE has been reported to enhance MMP-9 expression in myeloma cells [5, 6]. In our case, to distinguish whether the expressional up-regulation of MMPs is associated with the HPSE-mediated

shedding of the ECM and the related release of factors such as VEGF we performed blocking studies applying heparin [28, 39]. Since blockage of the extracellular activity of HPSE by heparin was not able to up-regulate the expression of MMPs (Supplementary Fig. S1B), we conclude that the regulatory effect depends on the nuclear function of HPSE. Recent studies which focused on HPSE activity in human malignant melanoma analyzed the extracellular shedding of the ECM and the associated release of prometastatic factors such as VEGF [3, 14]. In contrast to the strong up-regulation of MMPs the present study also documented a reduced availability of VEGF due to an expressional down-regulation and more importantly an impaired shedding of the ECM upon the down-regulation of HPSE (Fig. 2G, H). These data clearly indicate a dual function of HPSE in human melanoma cells comprising an intrinsic gene regulatory effect as well as an extracellular activity.

The pathophysiological relevance of HPSE on VEGF and MMP regulation was further confirmed in our tumor tissues. The microvessel density was reduced in tumor sections together with the attenuated VEGF availability, indicating that HPSE is highly involved in tumor angiogenesis, a pivotal step for tumor growth and spreading (Fig. 5B-D). Increased microvessel density was found correlating with up-regulation of HPSE in the previous studies, which was attributed to the proangiogenic property of HPSE [14, 37]. Compared to siCon group, siHPSE transfected tumors exhibited significantly enhanced MMP activities (Fig. 6C). Intriguingly, HPSE knockout mice was reported to exhibit elevated expression of MMP family members such as MMP-2, MMP-9 and MMP-14, in an organ-dependent manner suggesting a kind of compensation for HPSE deficiency [40]. Although HPSE deficiency was associated with an impaired primary tumor growth, our data showed an increased rate of lymph node metastasis together with a tendency of decreased survival rate (Fig. 6A, B). However, we also found a marked reduction of lung metastatic foci in mice receiving siHPSE cells via intravenous injection (Supplementary Fig. S5C), in line with the published data [32]. The complexity in terms of regulation and function prevents a straightforward interpretation

of experimental results. It may suggest that a different molecular mechanism affecting tumor metastasis formation may involve in our intradermal animal model, mainly depending on the local tumor microenvironment change. Interestingly, we identified increase amount of TNF-α, IL-1a, IL-2 and RANTES in tumor tissues upon HPSE knockdown (Supplementary Fig. S6F). Those proteins are known as strong indicators of inflammation which might contribute to the impaired survival rate.

MMP-9 expression is known to be transcriptionally regulated through activation of NF-κB signal transduction pathway [7, 8]. Moreover, it has been reported that NF-κB activation up-regulates HPSE expression in several tumors [9-12]. Therefore, we further investigated the relationship between HPSE and NF-κB in melanoma cells. Knockdown of HPSE significantly induced the expression of TNF-α, TF and PTX-3, all known as NF-κB-related products [41-43]. In addition, immunostainings and western blot analysis revealed increased amount of nuclear NF-κB upon HPSE knockdown in human malignant melanoma cells. These data strongly suggest a close relationship between HPSE and NF-κB. Of note, the relationship between HPSE and NF-κB is under controversial. Previous data reported that NF-κB activation up-regulates HPSE expression in several tumours [9-12]. Recently, focusing on the regulatory relationship between HPSE and NF-κB in glioblastoma cells, questioned their connection [44]. However, in the present study, we found that HPSE expression was inhibited upon activation of NF-κB by exogenous TNF-α stimulation in human melanoma cells (Supplementary Fig. S3D-F). This further confirms the mechanistic connection between HPSE and NF-κB.

HPSE has been shown to colocalize with nuclear HS in the nucleus of cancer cells [4, 45, 46]. In agreement, our data clearly prove the nuclear localization of HPSE in melanoma cells (Supplementary Fig S2A). Therefore, we hypothesized that the direct interaction between HPSE and DNA may explain the interference with NF-κB pathway. Actually, the direct interaction of HPSE with DNA has been speculated earlier [46] and has been now proven for the first time by high resolution atomic force microscopy (Fig. 4B-E). Co-precipitation of HPSE

and genomic DNA indicates a direct molecular interaction. We could further provide evidence that the interaction between HPSE and DNA is charge-driven and is non-specific which potentiates the involvement of other signaling pathway (Fig. 4F). This is in line with the up-regulation of MMP-2 which is not NF-κB-related. A schematic model shown in Figure 7 summarizes the main results of our study.

The mechanisms described here emphasize a close connection between HPSE, MMPs and VEGF. Due to a high degree of complexity the putative relevance and/or crucial contribution of each described pathway in patients is not yet predictable. In the past, the only selective regulation of VEGF, MMPs or HPSE was found to be contradictory [47, 48] indicating interactive molecular mechanism of tumor progression far beyond our current knowledge.

In conclusion, our data illustrate the duality of HSPE function. While nuclear HPSE interferes with the regulation of gene transcription by interaction with DNA, shedding of the ECM is related to the release of VEGF and thereby modulation of the vessel formation in the tumor. As a consequence, patients benefit is likely dependent on the tumor cell-specific behaviour and the associated ratio between VEGF availability and expressional regulation of pro-metastatic factors such as MMPs. These findings are novel and contribute to a more comprehensive understanding of HPSE in the course of protein expression and tumor cell progression, thus providing new insights into therapeutic strategies. Guided also by the clinical observation of a tumor suppressive function of nuclear HPSE in head and neck cancer [18], we propose the deliverance of HPSE into the nuclei of melanoma cells in combination with an inhibition of its extracellular activity may represent the most beneficial therapeutic concept.

Materials and Methods

Antibodies and Reagents

Polyclonal rabbit anti-human HPA1 (sc-25825), monoclonal mouse anti-human NF-κB p65 (sc-8008) antibodies were purchased from Santa Cruz Biotechnology (Santa Cruz, CA). Monoclonal mouse anti-β-actin antibodies were purchased from Sigma-Aldrich (Saint Louis, MO). Monoclonal mouse anti-human heparanase-1 antibodies (mAb 130) were purchased from Insight Biopharmaceuticals Ltd. (Rehovot, Israel). Polyclonal rabbit anti-human VEGF antibodies were purchased from Cell Sciences (Canton, MA). Polyclonal rabbit anti-mouse VEGF antibodies were purchased from Santa Cruz Biotechnology (Santa Cruz, CA). Monoclonal rat anti-mouse CD31 antibodies were purchased from BD Pharmingen™ (BD Biosciences, Heidelberg, Germany). Unfractionated heparin and recombinant human tumor necrosis factor-α (TNF-α) was purchased from Merck (Merck KGaA, Darmstadt, Germany).

Cell Culture

The human metastatic melanoma cell lines BLM, MV3 and IGR37 have been described previously [49-51] and were cultured in RPMI 1640 or Dulbecco's modified eagle medium (PAA, Pasching, Austria) supplemented with 10% fetal calf serum (FCS), 1% L-glutamine and 1% penicillin/streptomycin. Mouse B16F10 melanoma cells and *ret* transgenic melanoma cells [52, 53] were cultured in DMEM or RPMI 1640 medium supplemented with 10% fetal calf serum (FCS) and 1% L-glutamine. The high-resistance C7 subclone of Madin-Darby canine kidney cells (MDCK-C7) [54] were cultured in supplemented MEM medium (PAA, Pasching, Austria). All cells were cultured at 37°C in a humidified 5% CO_2/95% air atmosphere. Transfections were performed as previously described [22]. TEER measurements were done with MDCK-C7 cells as reported earlier [24].

Enzyme-linked Immunosorbent Assay

Released VEGF in melanoma cell supernatants was measured by a sandwich enzyme-linked immunosorbent assay (ELISA) technique following the manufacturer's protocol provided by DuoSet ELISA Development Kit (R&D, Minneapolis, MN) as previously described [22].

In Vivo Experiments

Mouse B16F10 or *ret* transgenic melanoma cells transfected with control siRNA or siHPSE vectors (pRNAT-CMV3.1-Neo, GenScript USA Inc., USA) were inoculated as cell suspension (7.5×10^5 cells/100 µl PBS) intradermally to the dorsal skin of 10-week old female C57BL/6 mice (n = 7). Xenograft size was determined every two days using a caliper. Tumor volume (V) was calculated with $V=0.5LW^2$, where *L* is the length and *W* the width of the xenograft. After four weeks, mice were sacrificed and xenografts were resected, weighted, and fixed in Tissue-Tek® (Sakura Finetek, Germany) for cryosectioning. Lymph nodes of inguinal, axillary and mandibular were collected and macroscopic pictures were documented.

For the analysis of lung metastasis formation, mice were intravenously (i.v.) injected with B16F10 cells (1.5×10^5) and euthanized after 14 days as described [32]. Metastatic foci were counted and macroscopic pictures of lungs were documented. Statistics was done using Mann-Whitney test.

Magnetic resonance (MR) images were acquired on a 1.5 T clinical MR scanner (Symphony, Siemens Healthcare Diagnostics GmbH, Germany) using a home-built coil for radiofrequency excitation and detection, designed as a cylindrical volume resonator. Data from DCE-MRI was analyzed according to a pharmacokinetic two-compartment [55], using the Dynalab workstation (Fraunhofer Mevis, Bremen, Germany) to calculate *amplitude A* ([arbitrary units], associated with relative blood volume) [56].

Immunofluorescence Staining, Western Blot and Zymography

Immunofluorescence staining, western blot, gelatin gel zymography and *in situ* Zymography were performed as previously described [22, 23, 27].

Proteome Profiler Array

The Proteome Profiler Array was performed using Mouse Cytokine Array C1000 kit (RayBiotech) to measure the relative levels of proteins in melanoma tissue lysates. The assay was performed according to the manufacturer's instructions. Melanoma tissue lysates were prepared as previously described [27]. Tissue lysates were pooled and equal amounts of total protein (500 µg) were loaded to the array kit. Blot images were analyzed with ImageJ software.

Solid-phase oligonucleotide binding assay

Binding assay was performed in a 96-well plate (MaxiSorp, NuncTM, Thermo Fisher Scientific, Schwerte, Germany). Wells were coated with HPSE, BSA or Poly-L-lysine (1 ng/well) and subsequently incubated with biotinylated oligonucleotides (20 fmols/well) in incubation buffer (100 mM Tris, pH 7.5, 100 mM NaCl, 2 mM $MgCl_2$). Non-bound oligonucleotides were removed with incubation buffer. Prior to the colorimetric detection of biotin residues by horseradish-peroxidase (HRP) conjugated streptavidin, cavities were blocked with 1% bovine serum albumin in incubation buffer.

RNA Isolation and RT-qPCR

Total RNA was extracted with the RNeasy mini kit (Qiagen, Hilden, Germany). Quantitative real-time PCR was performed as previously described [22]. The PCR primer sets were designed as follows: Human HPSE Forward, 5'-TGGGTTCTCCAAAGCTTC-3' and Reverse, 5'-TTGATTCCTTCTTGGGATCG-3'; Human TNF-α Forward, 5'-

CCCCAGGGACCTCTCTCTAATC-3' and Reverse, 5'-GCTTGAGGGTTTGCTACAACATG-3'; Human β-actin Forward, 5'-AGAAAATCTGGCACCACACC-3' and Reverse, 5'-CCATCTCTTGCTCGAAGTCC-3'; Mouse HPSE Forward, 5'-GGTGGAACAGCTCCAACGCCC-3' and Reverse, 5'-CCCTCGAGGCTGACCGATGT-3'; Mouse VEGF-A Forward, 5'-GAAGGGAGAGGAGCCCGCCA-3' and Reverse, 5'-CGCATCAGCGGCACACAGGA-3'; Mouse MMP-2 Forward, 5'-TGAGCTGTGGACCCTGGGAGA-3' and Reverse, 5'-GTGGTGCCACACCAGCGGTAG-3'; Mouse MMP-9 Forward, 5'-CGAGTTGTGGTCGCTGGGCA-3' and Reverse, 5'-CCCAACTACGGTCGCGTCCAC-3'. The primer sets for human tissue factor (TF), VEGF-A, MMP-2, MMP-9, pentraxin-3 (PTX-3) and glyceraldehyde-3-phosphate dehydrogenase (GAPDH) were purchased from Qiagen company (QuantiTect primer assay, Qiagen, Hilden, Germany).

Atomic Force Microscopy

Recombinant HPSE (R&D systems, USA) was mixed at different molar ratios with DNA and incubated for 30 minutes at room temperature in buffer (25 mM Tris/HCl, 150 mM NaCl, 5 mM $CaCl_2$, 5 mM $MgCl_2$, pH 7.4). 2 µl of the HPSE-DNA complex solution was adsorbed to freshly cleaved mica for 1 minute. The surface was rinsed with 1 ml ultra-pure water and imaged by atomic force microscope (Nanowizard I, JPK instruments, Berlin, Germany). Images were taken in tapping mode at a frequency of 315 Hz applying a cantilever with a spring constant of 14 N/m (NSC35, Micromash, Tallinn, Estonia).

Statistical Analysis

All results are representative of at least three independent experiments. Data are expressed as mean ± SD. Except for where noted, comparisons between two groups were analyzed by two-tailed Student's t-test, and $p < 0.05$ was considered as statistically significant.

Conflict of Interest

The authors declare no conflict of interest.

Acknowledgements

We thank Katja Oehme for the excellent technical help and advice in DCE-MRI experiments. We acknowledge Prof. Viktor Umansky (Skin Cancer Unit, German Cancer Research Center (DKFZ), Heidelberg and Department of Dermatology, Venereology and Allergology, University Medical Center Mannheim, Ruprecht-Karl University of Heidelberg, Mannheim, Germany) for providing *ret* transgenic mouse melanoma cells. This work was supported by the Deutsche Forschungsgemeinschaft within the SFB/Transregio 23 (project A9 to S.W.S).

References

1 Elkin M, Ilan N, Ishai-Michaeli R, Friedmann Y, Papo O, Pecker I *et al*. Heparanase as mediator of angiogenesis: mode of action. FASEB J 2001; 15: 1661-1663.

2 Vlodavsky I, Miao HQ, Medalion B, Danagher P, Ron D. Involvement of heparan sulfate and related molecules in sequestration and growth promoting activity of fibroblast growth factor. Cancer Metastasis Rev 1996; 15: 177-186.

3 Roy M, Marchetti D. Cell surface heparan sulfate released by heparanase promotes melanoma cell migration and angiogenesis. J Cell Biochem 2009; 106: 200-209.

4 Zong F, Fthenou E, Wolmer N, Hollosi P, Kovalszky I, Szilak L *et al*. Syndecan-1 and FGF-2, but not FGF receptor-1, share a common transport route and co-localize with heparanase in the nuclei of mesenchymal tumor cells. PLoS ONE 2009; 4: e7346.

5 Purushothaman A, Hurst DR, Pisano C, Mizumoto S, Sugahara K, Sanderson RD. Heparanase-mediated loss of nuclear syndecan-1 enhances histone acetyltransferase (HAT) activity to promote expression of genes that drive an aggressive tumor phenotype. J Biol Chem 2011; 286: 30377-30383.

6 Purushothaman A, Chen L, Yang Y, Sanderson RD. Heparanase stimulation of protease expression implicates it as a master regulator of the aggressive tumor phenotype in myeloma. J Biol Chem 2008; 283: 32628-32636.

7 Bond M, Fabunmi RP, Baker AH, Newby AC. Synergistic upregulation of metalloproteinase-9 by growth factors and inflammatory cytokines: an absolute requirement for transcription factor NF-kappa B. Febs Lett 1998; 435: 29-34.

8 Farina AR, Tacconelli A, Vacca A, Maroder M, Gulino A, Mackay AR. Transcriptional up-regulation of matrix metalloproteinase-9 expression during spontaneous epithelial to neuroblast phenotype conversion by SK-N-SH neuroblastoma cells, involved in enhanced invasivity, depends upon GT-box and nuclear factor kappaB elements. Cell Growth Differ 1999; 10: 353-367.

9 Andela VB, Schwarz EM, Puzas JE, O'Keefe RJ, Rosier RN. Tumor metastasis and the reciprocal regulation of prometastatic and antimetastatic factors by nuclear factor kappaB. Cancer Res 2000; 60: 6557-6562.

10 Cao HJ, Fang Y, Zhang X, Chen WJ, Zhou WP, Wang H *et al*. Tumor metastasis and the reciprocal regulation of heparanase gene expression by nuclear factor kappa B in human gastric carcinoma tissue. World J Gastroenterol 2005; 11: 903-907.

11 Wu WJ, Pan CE, Liu QG, Meng KW, Yu HB, Wang YL *et al*. [Expression of heparanase and nuclear factor kappa B in pancreatic adenocarcinoma]. Nan Fang Yi Ke Da Xue Xue Bao 2007; 27: 1267-1270.

12 Wu W, Pan C, Meng K, Zhao L, Du L, Liu Q *et al*. Hypoxia activates heparanase expression in an NF-kappaB dependent manner. Oncol Rep 2010; 23: 255-261.

13 Gingis-Velitski S, Zetser A, Flugelman MY, Vlodavsky I, Ilan N. Heparanase induces endothelial cell migration via protein kinase B/Akt activation. J Biol Chem 2004; 279: 23536-23541.

14 Zetser A, Bashenko Y, Edovitsky E, Levy-Adam F, Vlodavsky I, Ilan N. Heparanase induces vascular endothelial growth factor expression: correlation with p38 phosphorylation levels and Src activation. Cancer Res 2006; 66: 1455-1463.

15 Ilan N, Elkin M, Vlodavsky I. Regulation, function and clinical significance of heparanase in cancer metastasis and angiogenesis. Int J Biochem Cell Biol 2006; 38: 2018-2039.

16 Barash U, Cohen-Kaplan V, Dowek I, Sanderson RD, Ilan N, Vlodavsky I. Proteoglycans in health and disease: new concepts for heparanase function in tumor progression and metastasis. FEBS J 2010; 277: 3890-3903.

17 Boyango I, Barash U, Naroditsky I, Li JP, Hammond E, Ilan N *et al*. Heparanase cooperates with Ras to drive breast and skin tumorigenesis. Cancer Res 2014; 74: 4504-4514.

18 Cohen-Kaplan V, Jrbashyan J, Yanir Y, Naroditsky I, Ben-Izhak O, Ilan N *et al*. Heparanase induces signal transducer and activator of transcription (STAT) protein phosphorylation: preclinical and clinical significance in head and neck cancer. J Biol Chem 2012; 287: 6668-6678.

19 Roy M, Reiland J, Murry BP, Chouljenko V, Kousoulas KG, Marchetti D. Antisense-mediated suppression of Heparanase gene inhibits melanoma cell invasion. Neoplasia 2005; 7: 253-262.

20 Liu XY, Tang QS, Chen HC, Jiang XL, Fang H. Lentiviral miR30-based RNA interference against heparanase suppresses melanoma metastasis with lower liver and lung toxicity. Int J Biol Sci 2013; 9: 564-577.

21 Liu X, Fang H, Chen H, Jiang X, Fang D, Wang Y *et al*. An artificial miRNA against HPSE suppresses melanoma invasion properties, correlating with a down-regulation of chemokines and MAPK phosphorylation. PLoS ONE 2012; 7: e38659.

22 Desch A, Strozyk EA, Bauer AT, Huck V, Niemeyer V, Wieland T *et al*. Highly invasive melanoma cells activate the vascular endothelium via an MMP-2/integrin alphavbeta5-induced secretion of VEGF-A. Am J Pathol 2012; 181: 693-705.

23 Kerk N, Strozyk EA, Poppelmann B, Schneider SW. The mechanism of melanoma-associated thrombin activity and von Willebrand factor release from endothelial cells. J Invest Dermatol 2010; 130: 2259-2268.

24 Zak J, Schneider SW, Eue I, Ludwig T, Oberleithner H. High-resistance MDCK-C7 monolayers used for measuring invasive potency of tumour cells. Pflugers Arch 2000; 440: 179-183.

25 Goerge T, Barg A, Schnaeker EM, Poppelmann B, Shpacovitch V, Rattenholl A *et al*. Tumor-derived matrix metalloproteinase-1 targets endothelial proteinase-activated receptor 1 promoting endothelial cell activation. Cancer Res 2006; 66: 7766-7774.

26 Ludwig T, Ossig R, Graessel S, Wilhelmi M, Oberleithner H, Schneider SW. The electrical resistance breakdown assay determines the role of proteinases in tumor cell invasion. Am J Physiol Renal Physiol 2002; 283: F319-327.

27 Bauer AT, Burgers HF, Rabie T, Marti HH. Matrix metalloproteinase-9 mediates hypoxia-induced vascular leakage in the brain via tight junction rearrangement. J Cereb Blood Flow Metab 2010; 30: 837-848.

28 Vlodavsky I, Abboud-Jarrous G, Elkin M, Naggi A, Casu B, Sasisekharan R *et al*. The impact of heparanese and heparin on cancer metastasis and angiogenesis. Pathophysiol Haemost Thromb 2006; 35: 116-127.

29 Fairbrother WJ, Champe MA, Christinger HW, Keyt BA, Starovasnik MA. Solution structure of the heparin-binding domain of vascular endothelial growth factor. Structure 1998; 6: 637-648.

30 Micheau O, Tschopp J. Induction of TNF receptor I-mediated apoptosis via two sequential signaling complexes. Cell 2003; 114: 181-190.

31 Gorzelanny C, Poppelmann B, Strozyk E, Moerschbacher BM, Schneider SW. Specific interaction between chitosan and matrix metalloprotease 2 decreases the invasive activity of human melanoma cells. Biomacromolecules 2007; 8: 3035-3040.

32 Hostettler N, Naggi A, Torri G, Ishai-Michaeli R, Casu B, Vlodavsky I *et al*. P-selectin- and heparanase-dependent antimetastatic activity of non-anticoagulant heparins. FASEB J 2007; 21: 3562-3572.

33 Carrer A, Moimas S, Zacchigna S, Pattarini L, Zentilin L, Ruozi G *et al*. Neuropilin-1 identifies a subset of bone marrow Gr1- monocytes that can induce tumor vessel normalization and inhibit tumor growth. Cancer Res 2012; 72: 6371-6381.

34 Jain RK. Normalizing tumor vasculature with anti-angiogenic therapy: a new paradigm for combination therapy. Nat Med 2001; 7: 987-989.

35 Sato T, Yamaguchi A, Goi T, Hirono Y, Takeuchi K, Katayama K *et al*. Heparanase expression in human colorectal cancer and its relationship to tumor angiogenesis, hematogenous metastasis, and prognosis. J Surg Oncol 2004; 87: 174-181.

36 Shinyo Y, Kodama J, Hongo A, Yoshinouchi M, Hiramatsu Y. Heparanase expression is an independent prognostic factor in patients with invasive cervical cancer. Ann Oncol 2003; 14: 1505-1510.

37 Kelly T, Miao HQ, Yang Y, Navarro E, Kussie P, Huang Y *et al*. High heparanase activity in multiple myeloma is associated with elevated microvessel density. Cancer Res 2003; 63: 8749-8756.

38 Murphy G, Nagase H. Progress in matrix metalloproteinase research. Molecular aspects of medicine 2008; 29: 290-308.

39 Vlodavsky I, Mohsen M, Lider O, Svahn CM, Ekre HP, Vigoda M *et al*. Inhibition of tumor metastasis by heparanase inhibiting species of heparin. Invasion Metastasis 1994; 14: 290-302.

40 Zcharia E, Jia J, Zhang X, Baraz L, Lindahl U, Peretz T *et al*. Newly generated heparanase knock-out mice unravel co-regulation of heparanase and matrix metalloproteinases. PLoS ONE 2009; 4: e5181.

41 Oeth PA, Parry GC, Kunsch C, Nantermet P, Rosen CA, Mackman N. Lipopolysaccharide induction of tissue factor gene expression in monocytic cells is mediated by binding of c-Rel/p65 heterodimers to a kappa B-like site. Mol Cell Biol 1994; 14: 3772-3781.

42 Coward WR, Okayama Y, Sagara H, Wilson SJ, Holgate ST, Church MK. NF-kappa B and TNF-alpha: a positive autocrine loop in human lung mast cells? J Immunol 2002; 169: 5287-5293.

43 Basile A, Sica A, d'Aniello E, Breviario F, Garrido G, Castellano M *et al*. Characterization of the promoter for the human long pentraxin PTX3. Role of NF-kappaB in tumor necrosis factor-alpha and interleukin-1beta regulation. J Biol Chem 1997; 272: 8172-8178.

44 Hong X, Nelson K, Lemke N, Kalkanis SN. Heparanase expression is associated with histone modifications in glioblastoma. Int J Oncol 2012; 40: 494-500.

45 Schubert SY, Ilan N, Shushy M, Ben-Izhak O, Vlodavsky I, Goldshmidt O. Human heparanase nuclear localization and enzymatic activity. Lab Invest 2004; 84: 535-544.

46 Doweck I, Kaplan-Cohen V, Naroditsky I, Sabo E, Ilan N, Vlodavsky I. Heparanase localization and expression by head and neck cancer: correlation with tumor progression and patient survival. Neoplasia 2006; 8: 1055-1061.

47 Kamba T, McDonald DM. Mechanisms of adverse effects of anti-VEGF therapy for cancer. Br J Cancer 2007; 96: 1788-1795.

48 Hua H, Li M, Luo T, Yin Y, Jiang Y. Matrix metalloproteinases in tumorigenesis: an evolving paradigm. Cell Mol Life Sci 2011; 68: 3853-3868.

49 Van Muijen GN, Cornelissen LM, Jansen CF, Figdor CG, Johnson JP, Brocker EB *et al*. Antigen expression of metastasizing and non-metastasizing human melanoma cells xenografted into nude mice. Clin Exp Metastasis 1991; 9: 259-272.

50 van Muijen GN, Jansen KF, Cornelissen IM, Smeets DF, Beck JL, Ruiter DJ. Establishment and characterization of a human melanoma cell line (MV3) which is highly metastatic in nude mice. Int J Cancer 1991; 48: 85-91.

51 Aubert C, Rouge F, Galindo JR. Tumorigenicity of human malignant melanocytes in nude mice in relation to their differentiation in vitro. J Natl Cancer Inst 1980; 64: 1029-1040.

52 Hart IR. The selection and characterization of an invasive variant of the B16 melanoma. Am J Pathol 1979; 97: 587-600.

53 Kimpfler S, Sevko A, Ring S, Falk C, Osen W, Frank K *et al*. Skin melanoma development in ret transgenic mice despite the depletion of CD25+Foxp3+ regulatory T cells in lymphoid organs. J Immunol 2009; 183: 6330-6337.

54 Gekle M, Wunsch S, Oberleithner H, Silbernagl S. Characterization of two MDCK-cell subtypes as a model system to study principal cell and intercalated cell properties. Pflugers Arch 1994; 428: 157-162.

55 Brix G, Semmler W, Port R, Schad LR, Layer G, Lorenz WJ. Pharmacokinetic parameters in CNS Gd-DTPA enhanced MR imaging. J Comput Assist Tomogr 1991; 15: 621-628.

56 Merz M, Komljenovic D, Zwick S, Semmler W, Bauerle T. Sorafenib tosylate and paclitaxel induce anti-angiogenic, anti-tumour and anti-resorptive effects in experimental breast cancer bone metastases. Eur J Cancer 2011; 47: 277-286.

Figure 1. Knockdown of HPSE reduces melanoma cell invasive capacity

(A) Western blot analysis of HPSE protein level of human melanoma cells upon siRNA transfection. **(B)** Densitometry analysis of normalized HPSE protein levels by HPSE knockdown. White bar: siCon transfected; black bar: siHPSE transfected. **, $p < 0.01$. **(C)** RT-qPCR analysis of HPSE gene expression of siRNA transfected human melanoma cells. White bar: siCon transfected; black bar: siHPSE transfected. **, $p < 0.01$. **(D)** The schematic sketch of the experimental setup of TEER measurements. **(E)** Time course of TEER measurements of siRNA transfected human melanoma cells. Melanoma cells were added at day 0. White circle: siCon transfected; grey circle: siHPSE transfected; black circle: medium control. *, $p < 0.05$. **(F)** Normalized results of the TEER measurements. Points in X-axis reflect the time after tumor cell inoculation. White bar: siCon transfected; grey bar: siHPSE transfected; black bar: medium control. NS: no significant difference; **, $p < 0.01$.

Figure 2. Knockdown of HPSE enhances MMPs expression but reduces VEGF availability

(A) Gelatin gel zymography analysis of MMP-9 activity of human melanoma cells upon siRNA transfection. **(B)** Densitometry analysis of the MMP-9 zymography results. White bar: siCon transfected; black bar: siHPSE transfected. **, $p < 0.01$. **(C)** Gelatin gel zymography analysis of MMP-2 activity of siRNA transfected human melanoma cells. **(D)** Densitometry analysis of the MMP-2 zymography results. White bar: siCon transfected; black bar: siHPSE transfected. NS: no significant difference; **, $p < 0.01$. **(E-F)** RT-qPCR analysis of MMP-9 **(E)** and MMP-2 **(F)** gene expression of melanoma cells by siRNA transfection. White bar: siCon transfected; black bar: siHPSE transfected. *, $p < 0.05$; **, $p < 0.01$; NS: no significant difference. **(G)** VEGF ELISA analysis of cell supernatants harvested from transfected human melanoma cells. White bar: siCon transfected; black bar: siHPSE transfected. NS: no significant difference; **, $p < 0.01$. **(H)** Immunofluorescence stainings of VEGF (green) and glycocalyx (red) of transfected human melanoma cells. Scale bar corresponds to 20 µm.

Figure 3. HPSE is associated with nuclear factor kappa B in human melanoma cells

(A-C) RT-qPCR analysis of TNF-α **(A)**, tissue factor (TF) **(B)**, and pentraxin-3 (PTX-3) **(C)** gene expression of siRNA transfected human melanoma cells. White bar: siCon transfected; black bar: siHPSE transfected. *, $p < 0.05$; **, $p < 0.01$; NS: no significant difference. **(D)** Left panel: Western blot analysis of NF-κB p65 protein level in the cytosolic and nuclear extracts of human melanoma cells upon HPSE knockdown; right panel: Densitometry analysis of normalized nuclear NF-κB p65 protein levels by HPSE knockdown. White bar: siCon transfected; black bar: siHPSE transfected. **, $p < 0.01$. **(E)** Left panel: Immunofluorescence stainings of NF-κB p65 (red) of transfected human melanoma cells. Scale bar corresponds to 20 μm; right panel: Normalized nuclear fluorescence intensity levels upon HPSE knockdown. White bar: siCon transfected; black bar: siHPSE transfected. *, $p < 0.05$.

Figure 4. Molecular interaction between DNA and HPSE

(A) Western blot analysis probing HPSE co-precipitated with nuclear DNA. DNA was incubated either with low or high concentrations of sodium chloride prior to the precipitation. **(B-E)** Two dimensional (upper panel) and three-dimensional (lower panel) images obtained by atomic force microscopy of single HPSE **(B)**, single plasmid DNA **(C)**, and complexes formed from DNA and HPSE mixed at a molar ratios of 0.16 pmol HPSE to 0.03 pmol DNA **(D)** and at a molar ratio of 1.6 pmol HPSE to 0.03 pmol DNA **(E)**. White and black scale bars correspond to 50 nm. **(F)**. Binding of biotin-tagged NF-κB consensus oligonucleotides or randomized oligonucleotides to surface immobilized HPSE. BSA was used as a negative control while positively charged poly-L-lysine served as a positive control. NS: no significant difference.

Figure 5. Knockdown of HPSE inhibits B16F10 xenograft growth as well as angiogenesis

(A) Tumor volume of mice inoculated with control siRNA or HPSE siRNA transfected B16F10 melanoma cells (n=7). White circle: siCon transfected; black circle: siHPSE transfected. *, $p < 0.05$. **(B)** Left panel: Immunofluorescence stainings of VEGF (red) of tumor cryosections produced by either control siRNA or HPSE siRNA transfected B16F10 melanoma cells (n=6). Scale bar corresponds to 20 µm; right panel: Normalized fluorescence intensity levels of VEGF staining. **, $p < 0.01$. **(C)** Immunofluorescence stainings of CD31 (red) of tumor cryosections. Mosiac images, composed of 48 single images, are taken from at least 12 fields of 6 different xenografts. Scale bar corresponds to 500 µm. **(D)** Microvessel numbers counted in tumor xenografts of at least 12 independent tumor sections of 6 different xenografts. **, $p < 0.01$. **(E)** Color-coded maps for the parameter amplitude A (relative blood volume in the tumor) from DCE-MRI (left panel) and the corresponding quantification (right panel) (n=5).

Figure 6. Knockdown of HPSE reduces mouse survival but induces MMP activity

(A) Mice were inoculated with control siRNA or HPSE siRNA transfected B16F10 melanoma cells. Lymph nodes of inguinal, axillary and mandibular were collected and macroscopic pictures were documented (left panel). Analysis of mice with lymph node metastasis or not was listed as bar graph (right panel) (n=7). **(B)** Survival analysis of mice inoculated with control siRNA or HPSE siRNA transfected B16F10 melanoma cells (n=7). Solid line: siCon transfected; dashed line: siHPSE transfected. **(C)** *In situ* zymography analysis of gelatinase activity of tumor cryosections from mice inoculated with control siRNA or HPSE siRNA transfected B16F10 melanoma cells (n=6). Scale bar corresponds to 20 µm. **(D)** RT-qPCR analysis of MMP-2 gene expression of transfected B16F10 melanoma cells. **, $p < 0.01$. **(E)** Left panel: Immunofluorescence stainings of NF-κB p65 (red) of tumor cryosections produced by either control siRNA or HPSE siRNA transfected B16F10 melanoma cells (n=6). Scale bar corresponds to 20 µm; right panel: Normalized ratio of nuclear-to-cytosolic NF-κB p65 fluorescence intensity. NS: no significant difference.

Figure 7. Schematic model of the current study

The cytoplastic HPSE are released to the extracellular space and exert the enzymatic activity to shed the the heparan sulfate (HS) of the ECM. The HS-bound cytokines and molecules including VEGF get released and promote tumor vascularisation and thus growth of tumor. As an inhibitor of HPSE, Heparin can partially inhibit this effect. The nuclear HPSE inhibits NF-κB transcriptional activity by competing the binding to DNA thus preventing downstream genes expression, such as MMP-9. This regulatory effect is independent of HPSE enzymatic activity. MMPs are ECM-degrading enzymes which facilitate tumor cell extravasation as well as intravasation and thus enhance metastasis formation.

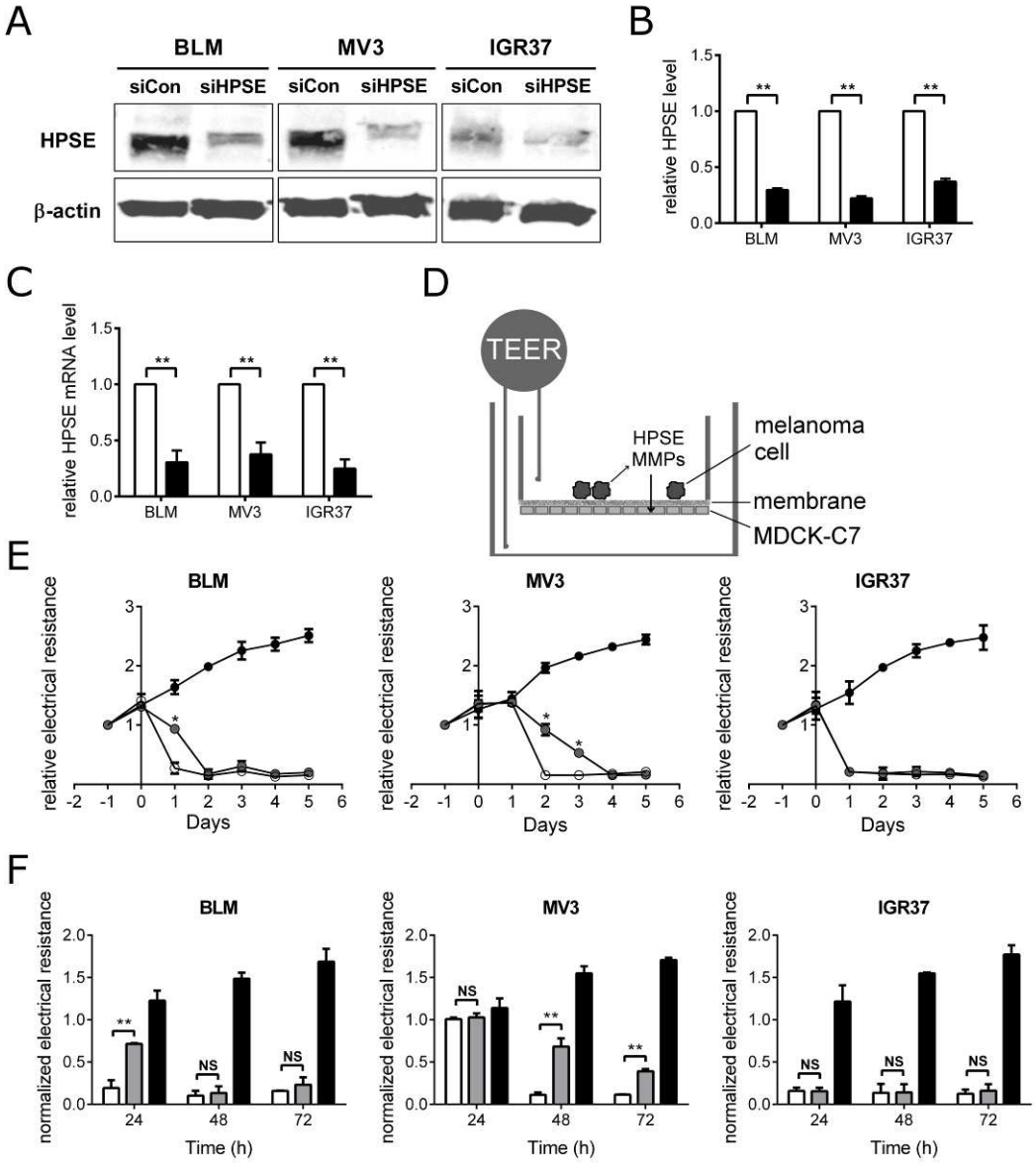
A
BLM
MV3
IGR37
siCon
siHPSE
HPSE
β-actin
B
relative HPSE level
C
relative HPSE mRNA level
D
TEER
HPSE
MMPs
melanoma
cell
membrane
MDCK-C7
E
relative electrical resistance
Days
F
normalized electrical resistance
Time (h)
NS

Figure 1

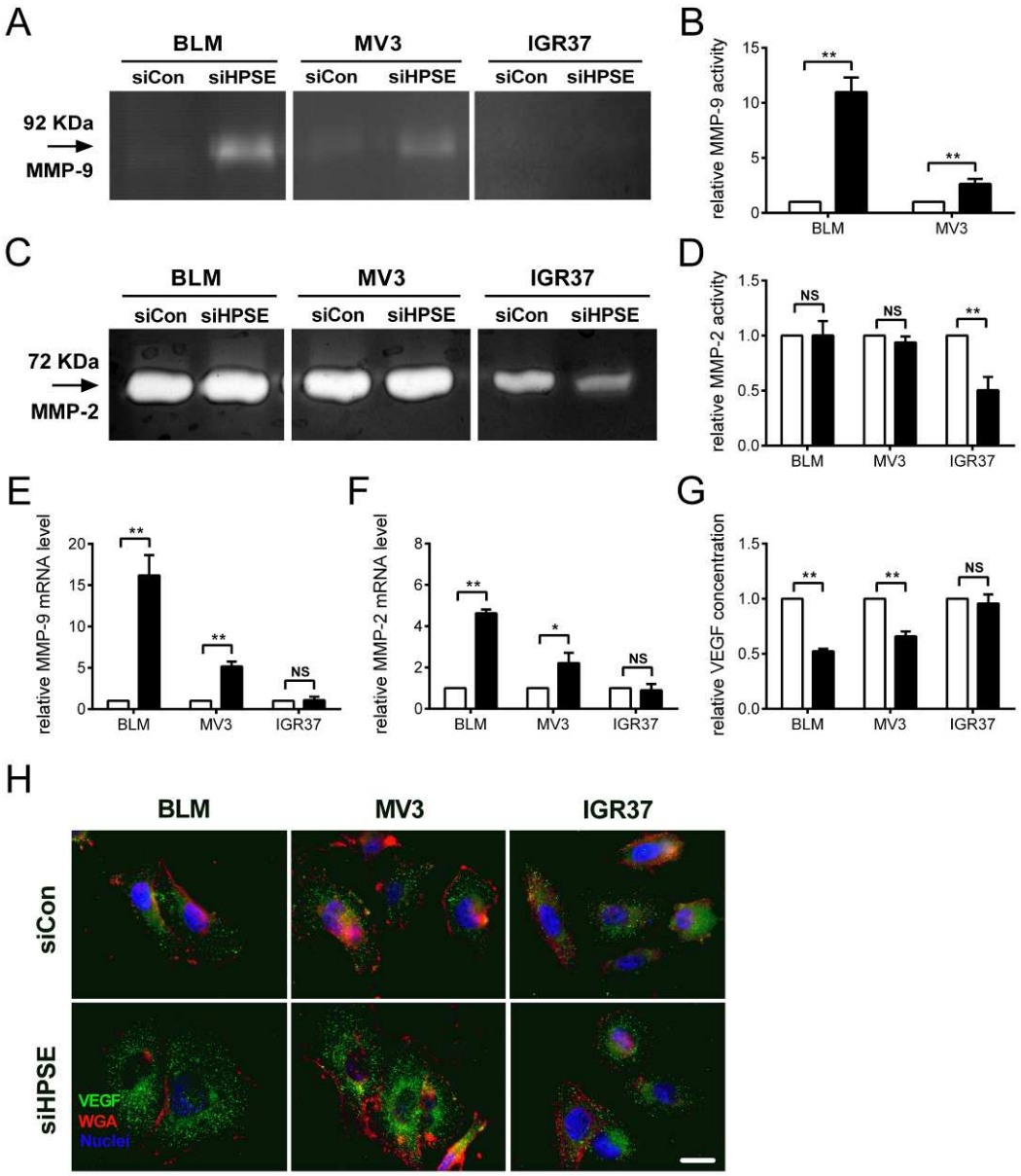
A
BLM
MV3
IGR37
siCon
siHPSE
92 KDa
MMP-9
B
relative MMP-9 activity
C
72 KDa
MMP-2
D
relative MMP-2 activity
NS
E
relative MMP-9 mRNA level
F
relative MMP-2 mRNA level
G
relative VEGF concentration
H
siCon
siHPSE
VEGF
WGA
Nuclei

Figure 2

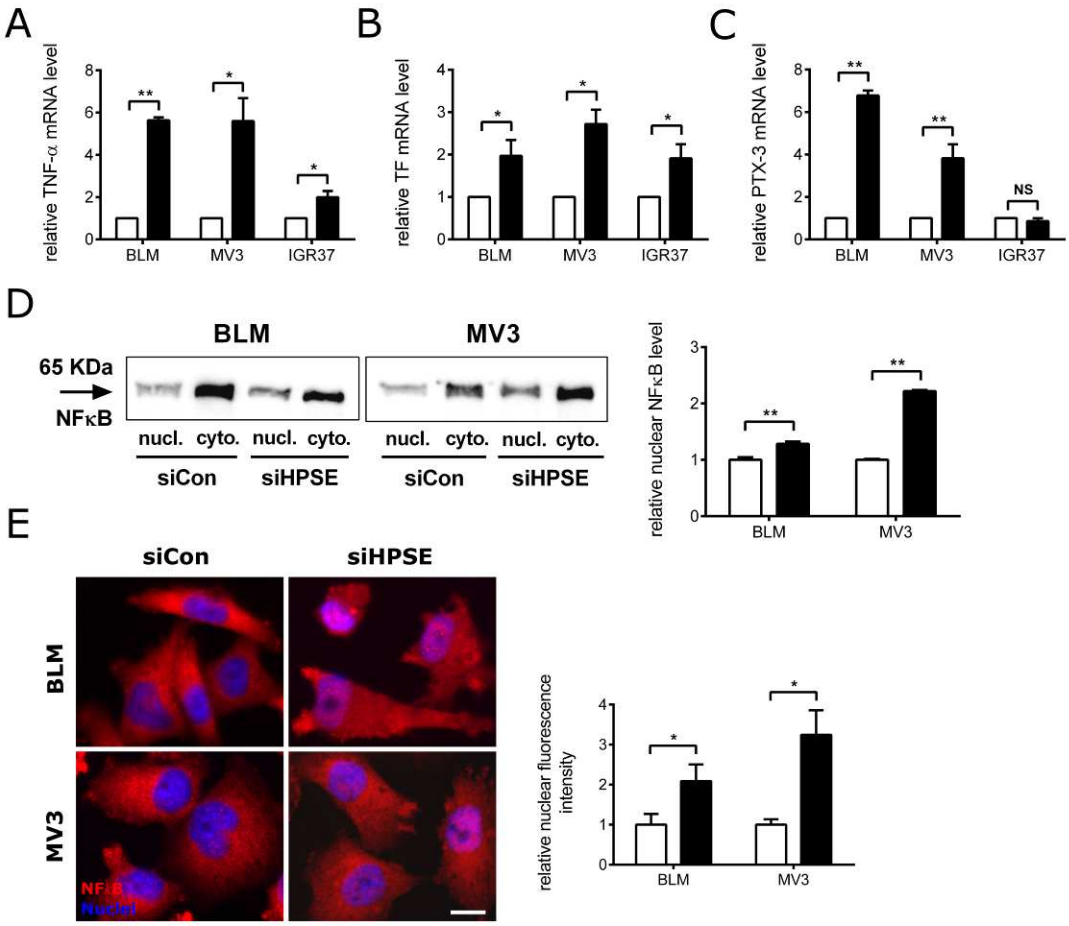

Figure 3

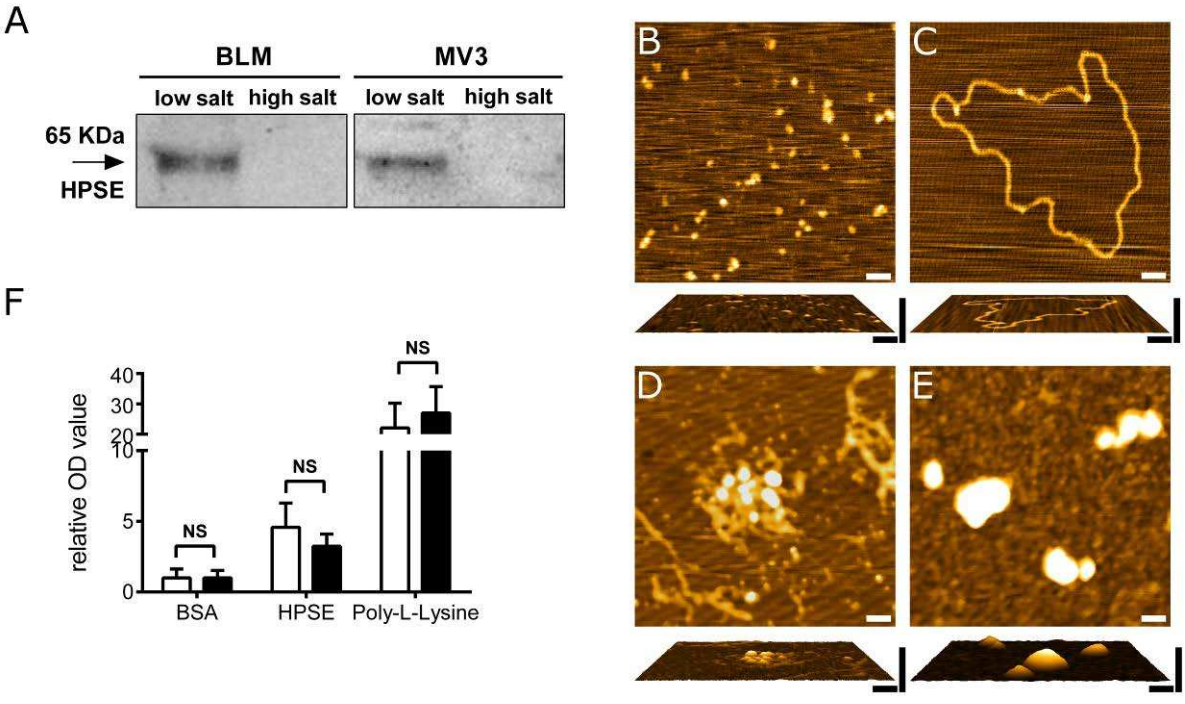

Figure 4

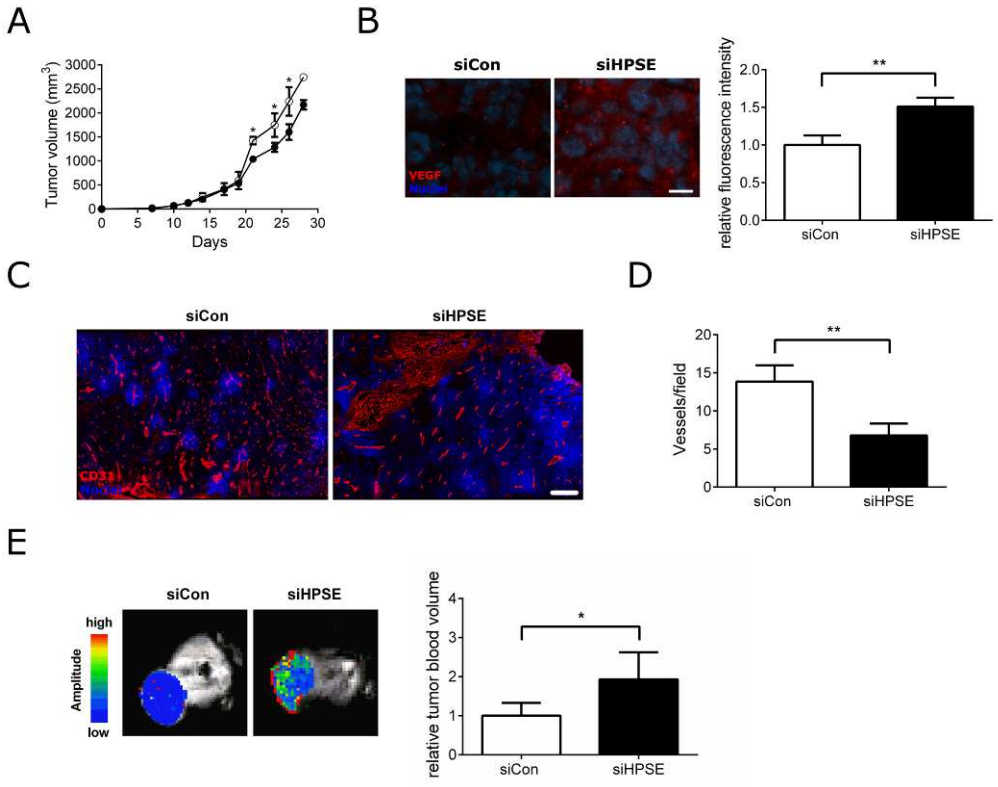

Figure 5

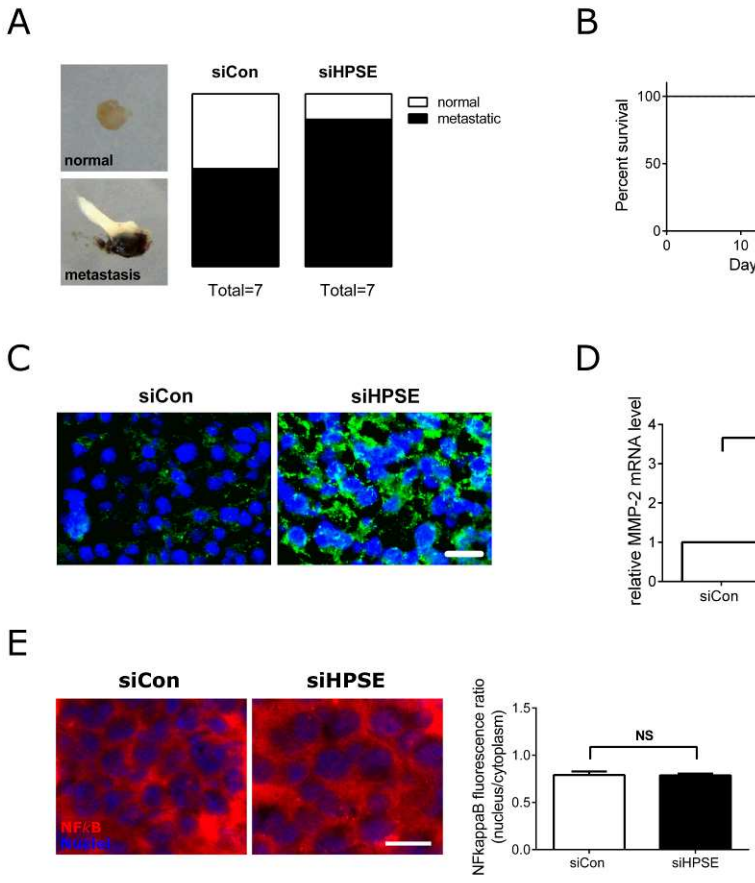

Figure 6

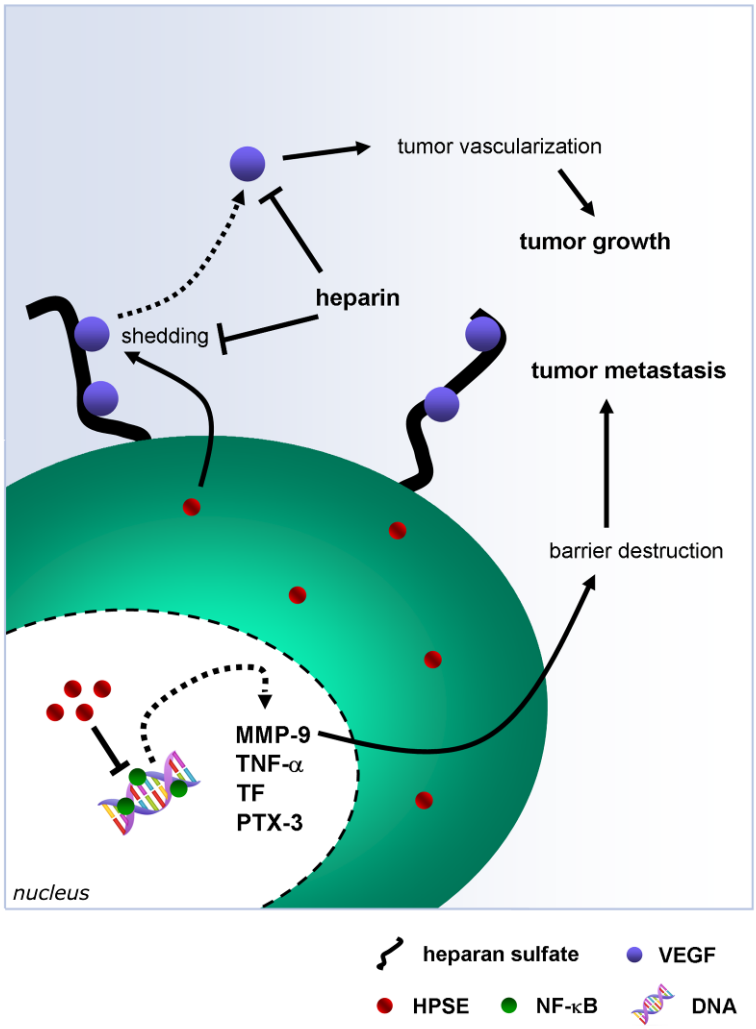
tumor vascularization
tumor growth
heparin
shedding
tumor metastasis
barrier destruction
MMP-9
TNF-α
TF
PTX-3
nucleus
heparan sulfate
VEGF
HPSE
NF-κB
DNA

Figure 7